2023 IEEE 6th Student Conference on Electric Machines and Systems (SCEMS) | 979-8-3503-2934-6/23/$31.00 ©2023 IEEE | DOI: 10.1109/SCEMS60579.2023.10379396

EMI Issues and Reduction in 800 V Electrical Vehicle Systems by Incorporating Cable Effects

1st Yuchen He
Center for advanced systems (CAPS)
Florida State University
Tallahassee, USA
yh19@fsu.edu

2nd Jinli Zhu
Center for advanced systems (CAPS)
Florida State University
Tallahassee, USA
jz23h@fsu.edu

3rd Bokang Zhou
Center for advanced systems (CAPS)
Florida State University
Tallahassee, USA
bzhou@fsu.edu

4th Xing Zhao
School of Physics, Engineering and Technology
University of York
York, United Kingdom
xing.zhao@york.ac.uk

***Abstract*—As electric vehicles (EVs) evolve, there is a notable shift in battery voltage levels from the conventional 400V to an elevated 800V. This transition offers advantages such as faster charging times, reduced energy losses, and the potential for more compact motor designs. However, this comes with a trade-off: an increased rate of voltage change (dv/dt), which can exacerbate Electromagnetic Interference (EMI) issues. The presence of cables connecting the motor to the motor drive and battery packs can further amplify these EMI challenges. Therefore, this paper initially conducts a comparative analysis of EMI performance between 400 V and 800 V EV systems. Subsequently, we introduce a filter design methodology specifically tailored to mitigate EMI in 800V bus systems. The efficacy of the proposed filter design is substantiated through both simulations and experimental results, confirming its role in effective EMI reduction with 20 dB reduction.**

***Index Terms*—EMI, EV, filters, cable effects**

I. Introduction

A. Prior Arts and Identified Challenges

EVs face two primary obstacles: extended charging durations and limited driving ranges. Compared to traditional 400-V systems, 800-V EV architectures offer distinct advantages, including accelerated charging rates, reduced energy losses, and the potential for high power density motors [1]. Consequently, 800-V systems are emerging as a promising alternative and likely future trend. While EMI has been recognized as a significant concern in EVs, existing research predominantly concentrates on subcomponent-level issues. These include the EMI characteristics of on-board chargers, inverters, and motors. However, the comprehensive EMI performance of an EV system, spanning from the battery to the inverter and motor drive, has received limited attention. Furthermore, specific EV designs, such as the Tesla Model Y, employ long cables to connect the battery to the motor drive. These extended cables effectively function as LC networks, potentially inducing resonance phenomena that can exacerbate existing EMI issues [2]–[4].

In electric vehicle (EV) powertrains, inverters are critical components that control motor operation through pulse width modulation (PWM). This modulation results in alternating current (AC) terminal voltages that oscillate between the high and low extremes of the DC bus voltage, creating steep common-mode (CM) voltage transitions with significant dv/dt levels. These rapid voltage changes, in turn, induce leakage currents due to parasitic capacitances within the powertrain components, including the battery, inverter, cables, and motor. Such leakage currents can lead to electromagnetic interference (EMI), potentially disrupting the operation of electronic devices within the vehicle. The arrangement of the system's components plays a crucial role in defining parasitic elements and the paths of EMI noise, ultimately affecting the level of CM EMI noise within the system [5]–[7].

Prior research in this field has primarily focused on three areas concerning SiC-based powertrains for EVs. The first area delves into the noise source characteristics of SiC inverters. Compared to their IGBT counterparts, SiC inverters exhibit higher EMI noise due to their increased switching frequencies. They also possess significantly higher dv/dt ratios, leading to amplified EMI within the powertrain. Additionally, the switching processes of SiC MOSFETs, particularly during turn-off, contribute additional EMI noise [8]–[11]. The alternative method explores the pathways of EMI noise transmission, including components like cables and motors. Models for permanent magnet synchronous motors (PMSM) have been developed through direct measurement or analytical methods grounded in electric machine theory. Measurement-based models offer practical insights for simulating motor drive EMI but often lack transparent physical interpretations. Conversely, analytical models provide clear physical rationale and utilize numerical methods or electromagnetic field analysis to estimate

circuit parameters. The layout of cables in an EV's powertrain can significantly influence EMI noise distribution and the overall conducted emissions. Research has shown that factors such as cable length and shielding can greatly affect EMI, with various studies examining the distribution of CM noise currents and the effectiveness of different shielding approaches [12]–[14]. Another investigation concerns the mitigation of system EMI noise. Techniques for reducing conducted EMI noise have been reported and include filtering, cancelling, and balancing methods. The filtering approach involves integrating passive filters into the converter system to obstruct or redirect EMI noise. Active filters represent the cancelling technique, where they generate a counteractive signal to neutralize EMI noise. Lastly, the balancing technique employs a Wheatstone bridge configuration using passive components to minimize noise within the system [15]–[17].

B. Key Contributions of this Paper

The key contributions of this paper can be summarized as follows:

- **Comprehensive Analysis of EMI Challenges in 800-V Systems:** While 800-V EV systems offer numerous benefits, this study reveals that the elevated DC voltage levels introduce substantially greater EMI complications compared to conventional 400-V systems.
- **Innovative Filter Design Methodology with Cable Considerations:** In response to the heightened EMI issues in 800-V systems, this paper introduces a targeted EMI filter design methodology. The design not only optimizes EMI performance but also considers the physical constraints of the filter, all while accounting for the effects of cable lengths.
- **Validation of EMI Mitigation:** Utilizing both simulation models and real-world experiments, this study confirms that the proposed EMI filter yields a 20 dB reduction in EMI levels, thereby achieving compliance with prevailing EMI standards.

II. Worsening EMI Issues in 800 V EV Systems

Inverters operating at high frequencies are a fundamental requirement for traction motor control in electric vehicles, but this comes with the drawback of creating significant electromagnetic interference (EMI) due to swift switching operations coupled with inherent parasitic elements. EMI problems arise in both conducted and radiated forms, predominantly dispersing through the system's wiring. Voltage spikes at the inverter's output have the potential to shorten motor life by harming windings, insulation, and bearings. Additionally, the rapid change in voltage levels, or dv/dt, contributes to increased eddy currents and the skin effect, which impacts the motor cores and windings.

The adoption of more advanced semiconductor technologies, like IGBTs and MOSFETs, in modern inverters introduces even faster switching speeds, which may intensify these complications. As battery voltages rise, there is a corresponding increase in dv/dt values, presenting greater challenges, particularly with the emerging adoption of wide bandgap (WBG) semiconductors in power electronics, known for their quick switching capabilities. Employing dv/dt filters can mitigate some of the adverse effects on the motor; however, other components in the electronic environment, such as gate drivers, may still be vulnerable to the effects of these rapid transitions.

The common-mode current pathway of the EV systems is depicted in Fig. 1. In this setup, a Permanent Magnet Synchronous Machine (PMSM) serves as the motor drive, receiving power from both the battery and the inverter. The common-mode pathway to the ground is formed by the junction capacitance of the heatsink in the inverter, as well as the enclosure of the PMSM. Elevated DC-link voltage levels result in an increased rate of voltage change (dv/dt), thereby exacerbating EMI issues. This phenomenon is corroborated by our simulation results. Figs. 2 and 3 collectively demonstrate an escalation in current spikes within 800 V systems in the time domain. Further validation is provided in the frequency domain, where the EMI levels surpass the CISPR 25 Class B standard, commencing at 100 kHz. This violation is evident in Fig. 4.

The common-mode (CM) noise voltage source V_{CM0} as depicted in Fig. 1 can be described by the following equation:

$$V_{CM0} = \frac{V_{AN} + V_{BN} + V_{CN}}{3} \tag{1}$$

In terms of circuit theory, the voltage $V_{L_{comm}}$ at the common-mode Line Impedance Stabilization Network (LISN) can be presented as:

$$V_{L_{comm}} = -A_d \frac{Z_b}{Z_b + Z_{R_{comm}}} V_{CM0} \tag{2}$$

Here, $V_{L_{comm}}$ and V_{CM0} represent the Laplace transforms of $v_{L_{comm}}$ and v_{CM0}, respectively. The alternating current (AC) impedance $Z_{R_{comm}}$, the direct current (DC) impedance Z_b, and the voltage ratio A_d from $V_{L_{comm}}$ to V_b are given by:

$$Z_{R_{comm}} = \frac{1}{s(3C_b + \frac{C_{comm}}{2})} // \left(sL_d + Z_P // \frac{1}{s\frac{C_{comm}}{2}} \right) \tag{3}$$

$$Z_b = \frac{1}{s(3C_{sd} + \frac{C_{sq}}{2})} // \left(sL_q + Z_S // \frac{1}{s\frac{C_{sq}}{2}} \right) \tag{4}$$

$$A_d = \frac{V_{L_{comm}}}{V_b} = \frac{sL_d + Z_S}{sL_d + Z_S // \frac{1}{s\frac{C_{sq}}{2}}} \tag{5}$$

III. Principle of EMI Filter Design by Incorporating Cable Effects

This section is dedicated to offering a comprehensive, step-by-step guide for designing an EMI filter tailored for 800V EV systems by considering the cable effects. The design of a Common-Mode (CM) filter for motor drives is a critical

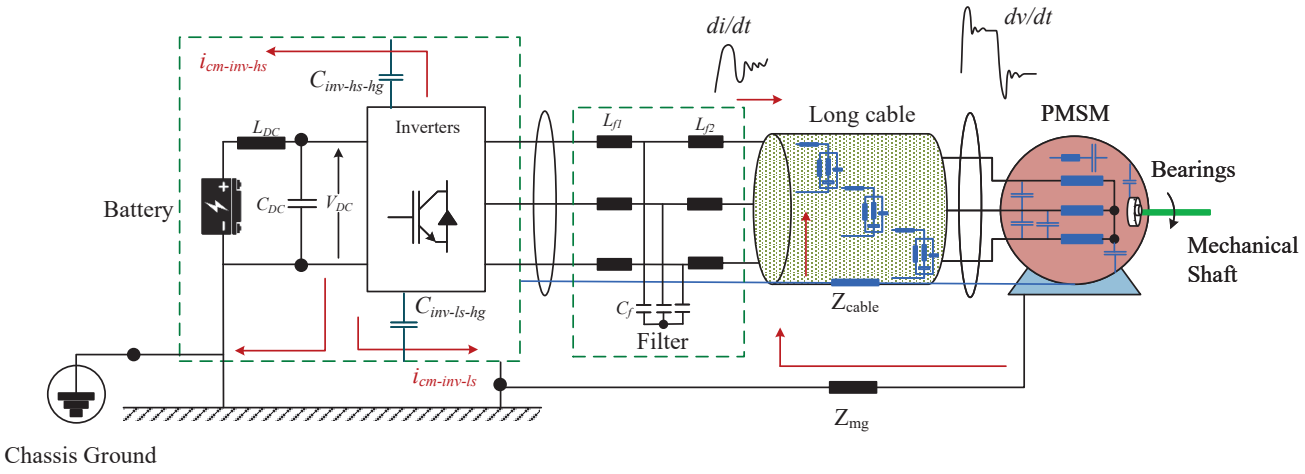

Fig. 1: Common mode current pathway in the 800 V EV systems

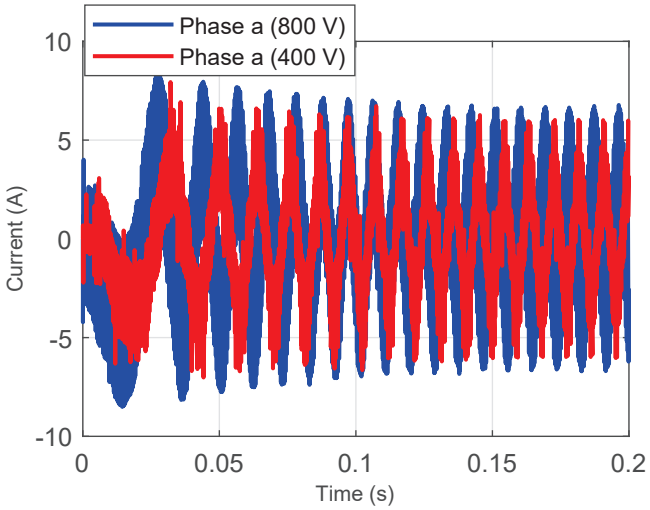

Fig. 2: Current waveforms for phase a current waveform under 800 V (blue line) and 400 V (red line).

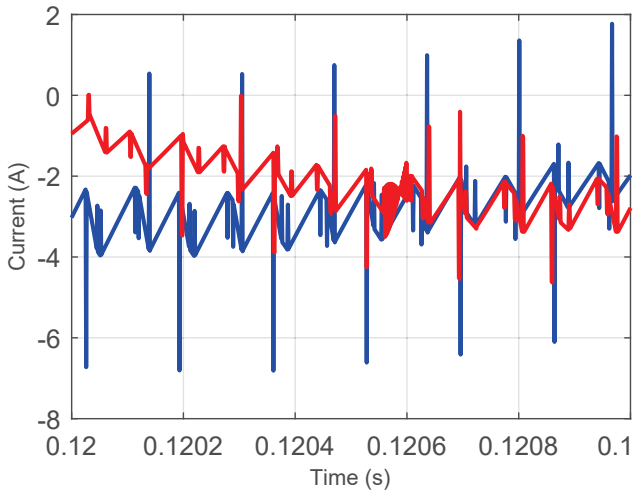

Fig. 3: Zoomed-in view of the phase a current waveform.

aspect to mitigate the CM voltage generated by the Pulse Width Modulated (PWM) rectifiers. This section delves into the configuration and selection of capacitors, their objectives, and the practical considerations for efficient CM filter design.

1) Filter Configuration: Capacitors C_{y1} and C_{y2} are deployed across the DC bus rails to prevent CM voltage escalation. The midpoint capacitor C_{Mg}, bridging the midpoint 'M' and ground, ensures that 'M' remains proximal to the ground potential.

2) Objective of Capacitors: The capacitors C_{y1} and C_{y2} constrain the flow of switching and lower-order frequency currents within the rectifier. Meanwhile, C_{Mg} lowers the resonance frequency to below the switching frequency, enhancing the stability and efficiency of advanced PWM techniques. The target is to maintain the third harmonic circulating current under 3% of the rated inductor current.

3) Selection of C_{Mg}: The capacitor C_{Mg} is chosen based on its role to attenuate high-frequency resonance and maintain low ground currents. The desired attenuation level is typically 95% to prevent significant voltage increase at point 'M'. The relationship governing C_{Mg} is given by:

$$\frac{V_{Mg}}{V_{Motor}} = \frac{C_{p2}}{C_{p1} + C_{Mg} + C_{p2}} \tag{6}$$

where V_{Mg} is the voltage at point 'M', and V_{Motor} is the average voltage of the Active Front End (AFE).

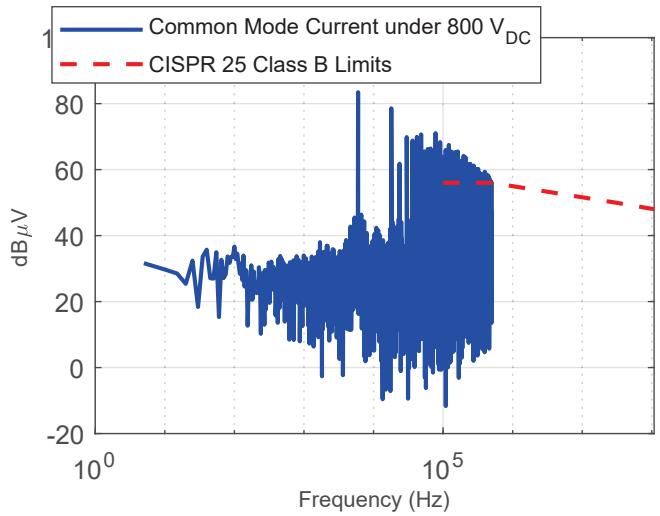

Fig. 4: EMI performance of common mode current against the CISPR 25 standard.

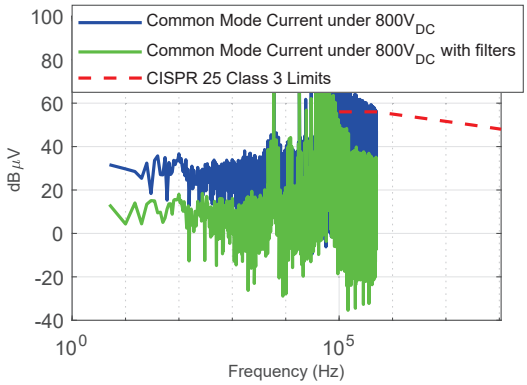

Fig. 5: EMI performance comparison between the 800 V case without filters and with added filters.

4) Design Criteria: The design process includes maintaining the resonance frequency below the switching frequency of the PWM rectifier, leading to the condition:

$$f_{res} < \frac{\omega_{sw}}{2\pi} < \frac{\omega_{sw}}{2} \tag{7}$$

where f_{res} is the resonance frequency and ω_{sw} is the switching angular frequency.

5) Impedance Matching at High Frequencies: To ensure proper operation at high frequencies, the inductive reactance of L_a and L_s become significantly high, effectively behaving as open circuits. The capacitive reactance hence dominates, necessitating precise selection of C_{y1} and C_{y2} for optimal impedance matching, as shown by:

$$\alpha = \left(\frac{1}{C_{y1}} + \frac{1}{C_{y2}} + \frac{1}{C_{Mg}} \right)^{-1} \tag{8}$$

6) Validation and Testing: The theoretical designs are substantiated through simulations and empirical testing to confirm the CM filter's performance under operational stresses.

This comprehensive design strategy ensures the CM filter's effectiveness in reducing noise and improving the electromagnetic compatibility of motor drives.

IV. Simulation and Experimental Results

Figure 5 showcases the efficacy of the implemented filter, represented by the green line. The filter achieves a substantial reduction in EMI noise, specifically by 20 dB above 100 kHz, which is the threshold frequency for CISPR standards. Consequently, the proposed filter enables the 800V system to comply with existing EMI regulations.

Parameter	Description	Default Value
L_q	q-axis inductance	3.2mH
R_s	Stator resistance	0.636Ω
R_{comm}	Common mode resistance	0.24 Ω
Z_b	Bearing impedance	2.25M Ω
Moment of Inertia	Moment of inertia	2e-4
L_d	d-axis inductance	0.66mH
Initial Rotor Angle	Initial rotor angle	0
$V_{\text{pk/krpm}}$	Peak line-to-line back EMF constant	45.3
Master/Slave Flag	Master-slave flag	1
C_s	Phase winding stray capacitance	1.1nF
No. of Poles P	Number of poles	4
R_b	Bearing resistance	10 Ω
Shaft Time Constant	Shaft time constant	5
L_{comm}	Common mode inductance	0.95mH
C_b	Bearing capacitance	185pF
C_{comm}	Common mode capacitance	7.3nF
C_{sd}	d-axis differential mode capacitance	2.1nF
C_{sq}	q-axis differential mode capacitance	1.7nF

TABLE I: Table of Parameters with Subscript Notation

V. Conclusions and Future Directions

This study serves as a preliminary investigation into EMI mitigation for 800V electric vehicle systems. While the proposed filter design has demonstrated promising results, future research will focus on providing a more nuanced analysis and conducting additional experimental validations to further optimize the system's EMI performance.

References

[1] Y. Yang, Q. Huang, Y. Lai, Z. Ma, Y. Liu and S. Wang, "Analysis and Modeling of the Near Magnetic Field Distribution of Toroidal Inductors," 2023 IEEE Symposium on Electromagnetic Compatibility and Signal/Power Integrity (EMC+SIPI), Grand Rapids, MI, USA, 2023, pp. 573-578, doi: 10.1109/EMCSIPI50001.2023.10241669.

[2] R. B. Gonzatti, B. Zhou, Y. He, A. R. Taylor and F. Peng, "Virtual Impedance-based Grid Synchronization for Converters Connected Through Long Cables," 2020 IEEE Energy Conversion Congress and Exposition (ECCE), Detroit, MI, USA, 2020, pp. 4512-4519, doi: 10.1109/ECCE44975.2020.9236016.

[3] Y. He, Y. Li, B. Zhou and F. Z. Peng, "Switching-Cycle-Based Startup for Grid-tied Inverters," 2023 IEEE 17th International Conference on Compatibility, Power Electronics and Power Engineering (CPE-POWERENG), Tallinn, Estonia, 2023, pp. 1-5, doi: 10.1109/CPE-POWERENG58103.2023.10227483.

[4] B. Zhou, Y. He, Y. Zou, Y. Li and F. Z. Peng, "An Inner-Loop Control Method for the Filter-less, Voltage Sensor-less, and PLL-less Grid-Following Inverter-Based Resource," 2022 IEEE Applied Power Electronics Conference and Exposition (APEC), Houston, TX, USA, 2022, pp. 1425-1429, doi: 10.1109/APEC43599.2022.9773557.

[5] M. Gao, H. L. Herrera and J. Moon, "Optimization of Core Size and Harvested Power for Magnetic Energy Harvesters based on Cascaded Magnetics," 2023 IEEE Applied Power Electronics Conference and Exposition (APEC), Orlando, FL, USA, 2023, pp. 2926-2932, doi: 10.1109/APEC43580.2023.10131308.
[6] Q. Yang et al., "A Nonlinear Inductor-Based Fault Current Commutation Strategy to Enable Zero-Current Opening of the Mechanical Switch in a Hybrid DC Circuit Breaker," 2023 IEEE Electric Ship Technologies Symposium (ESTS), Alexandria, VA, USA, 2023, pp. 498-504, doi: 10.1109/ESTS56571.2023.10220510.
[7] Y. He et al., "Control Development and Fault Current Commutation Test for the EDISON Hybrid Circuit Breaker," in IEEE Transactions on Power Electronics, vol. 38, no. 7, pp. 8851-8865, July 2023, doi: 10.1109/TPEL.2023.3262605.
[8] M. Gao, L. Yi and J. Moon, "Mathematical Modeling and Validation of Saturating and Clampable Cascaded Magnetics for Magnetic Energy Harvesting," in IEEE Transactions on Power Electronics, vol. 38, no. 3, pp. 3455-3468, March 2023, doi: 10.1109/TPEL.2022.3218725.
[9] M. Gao, L. Yi and J. Moon, "Analysis, Modeling, and Validation of Cascaded Magnetics for Magnetic Energy Harvesting," 2022 IEEE Energy Conversion Congress and Exposition (ECCE), Detroit, MI, USA, 2022, pp. 1-7, doi: 10.1109/ECCE50734.2022.9947560.
[10] Z. Ma, Y. Lai, Y. Yang, Q. Huang and S. Wang, "Review of Radiated EMI Modeling and Mitigation Techniques in Power Electronics Systems," 2023 IEEE Applied Power Electronics Conference and Exposition (APEC), Orlando, FL, USA, 2023, pp. 1776-1783, doi: 10.1109/APEC43580.2023.10131552.
[11] M. Gao, B. Song, Y. He "Comparison of the Mechanical Properties of Two Different Hybrid Circuit Breakers," in IEEE Transactions on Power Electronics, vol. 38, no. 4, pp. 4571-4583, April 2023, doi: 10.1109/TPEL.2022.3201923.
[12] R. B. Gonzatti, B. Zhou, A. R. Taylor, Y. He and F. Peng, "Effects of Cable Inductance on Grid-Synchronous Control of Converters," in IEEE Transactions on Industrial Electronics, vol. 70, no. 5, pp. 4420-4430, May 2023, doi: 10.1109/TIE.2022.3187759.
[13] Y. He, B. Zhou, Y. Li and F. Z. Peng, "Impedance Modeling and Stability Analysis for the PLL-less and Voltage Sensor-less Grid-tied Converters," 2023 IEEE 17th International Conference on Compatibility, Power Electronics and Power Engineering (CPE-POWERENG), Tallinn, Estonia, 2023, pp. 1-5, doi: 10.1109/CPE-POWERENG58103.2023.10227472.
[14] Q. Yang, B. Zhou, Y. He, "Fault Detection and Interruption for a DC Microgrid using a Hybrid Circuit Breaker," in IEEE Transactions on Smart Grid, vol. 14, no. 2, pp. 1262-1276, March 2023, doi: 10.1109/TSG.2022.3143928.
[15] R. B. Gonzatti, F. Z. Peng, A. R. Taylor, Y. He, "Optimal Virtual Impedance Setting for Voltage Source Converters in Microgrids," 2023 IEEE International Conference on Smart Grid Communications (SmartGridComm), Beijing, China, 2023, pp. 1-6, doi: 10.1109/SmartGridComm50501.2023.9985689.
[16] Y. He, B. Zhou, Y. Zou, Y. Li "A PLL-less Control Strategy for Power Converters in Microgrids with High Inductance Lines," 2023 IEEE Texas Power and Energy Conference (TPEC), College Station, TX, USA, 2023, pp. 1-6, doi: 10.1109/TPEC53508.2023.9958604.
[17] Y. He, B. Zhou, R. B. Gonzatti, F. Z. Peng "A Distributed Control Scheme for Power Converters in a Microgrid with Zero Steady-State Error," in IEEE Transactions on Power Systems, early access, 2023, pp. 1-13, doi: 10.1109/TPWRS.2023.3191109.